Proceedings of the Twenty-Ninth AAAI Conference on Artificial Intelligence

An Entorhinal-Hippocampal Model for Simultaneous Cognitive Map Building

Miaolong Yuan[1], **Bo Tian**[1], **Vui Ann Shim**[1], **Huajin Tang**[1,2,*], **Haizhou Li**[1]
[1]Institute for Infocomm Research, Agency for Science, Technology and Research (A*STAR), Singapore 138632
[2]College of Computer Science, Sichuan University, Chengdu, China 610065

Abstract

Hippocampal place cells and entorhinal grid cells have been hypothesized to be able to form map-like spatial representation of the environment, namely cognitive map. In most prior approaches, either neural network methods or only hippocampal models are used for building cognitive maps, lacking biological fidelity to the entorhinal-hippocampal system. This paper presents a novel computational model to build cognitive maps of real environments using both place cells and grid cells. The proposed model includes two major components: (1) A competitive Hebbian learning algorithm is used to select velocity-coupled grid cell population activities, which path-integrate self-motion signals to determine computation of place cell population activities; (2) Visual cues of environments are used to correct the accumulative errors intrinsically associated with the path integration process. Experiments performed on a mobile robot show that cognitive maps of the real environment can be efficiently built. The proposed model would provide an alternative neuro-inspired approach for robotic mapping, navigation and localization.

Introduction

Spatial cognition is the basic ability of mammals to perform cognitive tasks including exploration, map building, localization, and navigation in an environment. For decades, researchers have been investigating how animals perceive space and navigate freely in an environment. Tolman suggested that navigation is guided by an internal map-like representation, i.e., *cognitive map*, which represents the spatial relationship among salient landmarks of an environment (Tolman 1948).

Earlier studies of spatial cognition discovered that place cells and head direction cells in the rat hippocampus are involved in the development of abstract-level cognitive maps of spatial relations (O'Keefe and Dostrovsky 1971; O'keefe and Nadel 1978; Taube 2007). Place cells fire only when a rat occupies a specific location in a given environment and provide the rat with a dynamic, continuously updated representation of allocentric space, while head direction cells fire when the rat's head is at a specific global orientation. However, the discrete representations of individual place cell and head direction cell activity could not be sufficient to support navigation from one place to another. When rats move away from a start position, they can keep track of their relative changing positions by path-integrating linear and angular self-motion and return to their original location effortlessly (Moser, Kropff, and Moser 2008; Domnisoru, Kinkhabwala, and Tank 2013; McNaughton et al. 2006). The historical discovery of grid cells in the dorsocaudal medial entorhinal cortex (dMEC) strongly suggests that path integrator exists in the brain, as grid fields persist after removal or replacement of major landmarks points and self-motion information is regarded as the primary source for maintaining and updating grid representations (Hafting et al. 2005). Grid cells display strikingly regular firing responses to the animal's locations in 2-D space and provide metric information for mapping space. A widely held view is that grid cells path-integrate self-motion signals of speed and direction to update the place cell's firing fields, whereas external cues specifying location allow error correction associated with the path integration (Hafting et al. 2005; Milford, Wiles, and Wyeth 2010). It is unclear, however, how grid cells interact with place cells in the entorhinal-hippocampal system (Bonnevie et al. 2013). Existing studies suggested that place cell responses may be generated from a subset of grid cell inputs (McNaughton et al. 2006; Solstad, Moser, and Einevoll 2006; Monaco and Abbott 2011). Two main models have been proposed to account for the formation of place cell responses by (1) a linear summation of a subset of afferent grid cells with a range of spatial frequencies (Solstad, Moser, and Einevoll 2006; Fuhs and Touretzky 2006); and (2) competitive learning among grid cell inputs with various spacings and orientations (Rolls, Stringer, and Elliot 2006; Monaco and Abbott 2011).

It has also been found that rats have mechanisms to correct the accumulative errors of path integration when they meet salient landmarks (McNaughton et al. 2006). While many models (Solstad, Moser, and Einevoll 2006; Si and Treves 2009; Savelli and Knierim 2010) focus on how place cell responses are generated from grid cell inputs without considering coupling velocity information into grid cells, (Burak and Fiete 2009) proposed a grid cell model using continuous attractor network (CAN), which can per-

form accurate path integration with noise-free velocity inputs. However, their study still suffers from some major constraints. Firstly, the CAN-based grid cell model itself is insufficient to build a cognitive map, lacking the important recurrent interactions with place cells (Bonnevie et al. 2013). Secondly, it remains unknown whether the actual self-motion and visual inputs can drive a model for error corrections to construct cognitive maps.

In this work, we aim to develop a computational model integrating visual cues, place cells and velocity-coupled grid cells for building cognitive maps. We use one dimensional continuous attractor network (CAN) to model head direction cells, as in (McNaughton et al. 2006; Zhang 1996), to encode orientations of the robot and will not discuss it in detail. Our strategy is based on the principle that velocity-coupled grid cells play the role of path integrator while place cells encode the output of path integration (Moser, Kropff, and Moser 2008). To the best of our knowledge, this is the first model in which visual inputs, place cells and velocity-coupled grid cells contribute together to build spatial cognitive maps of indoor environments on a mobile robot.

Cognitive map mechanisms have continuously inspired important implications in robotic mapping and navigation. In (Burgess et al. 1997), the model was coupled strongly to the biology of place cells, and showed how place cell firing can enable mapping and navigation in a miniature mobile robot. Multimodal integration of visual place cells and grid cells was proposed to enhance robot localization (Cuperlier, Quoy, and Gaussier 2007; Jauffret, Cuperlier, and Gaussier 2012). Most models have been tested only in laboratory environments and cognitive maps have not been built in these models. RatSLAM (Milford and Wyeth 2008), made a significant progress in emulating the spatial navigation ability of the hippocampal system, being able to build a semi-metric topological map in a real large area. (Tian et al. 2013) extended to use an RGB-D sensor to built cognitive maps for robot navigation. However, path integration in these works was performed by a heuristic method that makes an appropriately displaced copy of place cell activities, which sacrifices biological fidelity.

In summary, this work makes the important progress in the following two aspects:

1. The proposed entorhinal-hippocampal model, in which place cells, velocity-coupled grid cells and visual inputs contribute together to building cognitive maps simultaneously, presents the closest biological fidelity. It provides an embodied substrate to verify neural activities of the entorhinal-hippocampal circuitry found in neurobiological experiments, e.g., in laboratory rats.

2. The spatial cognitive system built on a mobile robot provides a practical robotic mapping and navigation approach. It would motivate more practical developments on neuro-inspired robotic spatial cognitive systems in real environments.

Methods

Architecture

Figure 1 shows the system architecture to build cognitive maps on a mobile robot platform. The robot consists of a Pioneer 3-DX mobile base, an RGB-D sensor and a laptop with an Intel(R) Core(TM) i7-3740 CPU with 16GB RAM. The front wheels of the base are equipped with encoders that provide raw odometry data and the RGB-D sensor is mounted on the front-top of the base to capture visual RGB-D images of environments. The robot's locations and orientations are encoded in place cell and head direction cell population activities, respectively. The system includes four major steps: (1) Self-motion of the raw odometry data is used to generate and drive the velocity-coupled grid cell activities. (2) A Hebbian learning algorithm is applied to learn the strengths, i.e., the weights, between place cell and gird cell population activities and determine computation of place cell activities, which path-integrate self-motion during map building. (3) Visual images are used for correcting the accumulative errors associated with the path integration and resetting when loop closures are detected. (4) A cognitive map is updated during the building process.

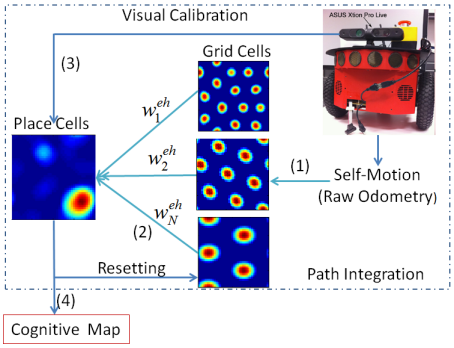

Figure 1: System architecture. Steps (1)-(4) are explained in text.

From Grid Cells to Place Cells

There are mainly two general models to describe grid cell formation, i.e., oscillatory interference (Burgess 2008; Zilli and Hasselmo 2010) and CAN (Fuhs and Touretzky 2006; Burak and Fiete 2009). In an oscillatory interference model, grid cells exhibit theta phase precession during the theta cycle, acutely vulnerable to subtle changes in the phase of underlying oscillation. In a CAN model, neurons are often arranged in a 2D neural sheet. Recurrent connectivity among the neurons in a neural sheet with a global inhibition leads random patterns of population activity to spontaneously merge to organized 'bumps' of grid cell population activity (Burak and Fiete 2009). The bumps are envisaged to move as the animal moves from one place to another. A grid cell response is obtained by summing the firing activity of a single neuron over a full trajectory. The most remarkable progress of (Burak and Fiete 2009) is to accurately integrate velocity inputs into grid cell models. In this work, we

use a simplified CAN model to generate and drive velocity-coupled grid cell population activities.

As in (Burak and Fiete 2009), the dynamics of rate-based neurons in a 2D neural sheet is specified by:

$$\tau ds_i/dt = \left[\sum_j W_{ij}^g s_j + B_i\right]_+ - s_i \quad (1)$$

where $[\cdot]_+$ denotes a threshold-linear function that leaves positive arguments unchanged and sets negative ones to zero. W_{ij}^g is the synaptic weight from neuron j to neuron i in a neural sheet. $\sum_j W_{ij}^g s_j$ is the inhibitory recurrent input to neuron i, s_i is the synaptic activation of neuron i and τ is the time-constant of neuron response. If the length of a neural sheet is n, there will be n^2 neurons in the network. Each neuron i has a preferred direction θ_i (W, N, S or E). The feed-forward excitatory input B_i to neuron i, defined by:

$$B_i = 1 + \alpha \hat{\mathbf{e}}_{\theta_i}.\mathbf{v}_t \quad (2)$$

where $\hat{\mathbf{e}}_{\theta_i}$ is the unit vector pointing to θ_i. $\mathbf{v}_t$ is the velocity at time t. W_{ij} is defined as follow:

$$W_{ij}^g = W_0^g(\mathbf{x}_i - \mathbf{x}_j - l\hat{\mathbf{e}}_{\theta_j}) \quad (3)$$

with

$$W_0^g = g_{exc}\mathbf{e}^{-\gamma|\mathbf{x}|^2} - \mathbf{e}^{-\beta|\mathbf{x}|^2} \quad (4)$$

where g_{exc} is the gain which modulates the size of grid cell population activities and l is the shift in the outgoing weights. λ determines the spacing of the activity in a neural sheet. We use $\gamma = 1.1\beta$, $\beta = 3\lambda^{-2}$.

As mentioned in (Fuhs and Touretzky 2006), one grid cell population activity in one neural sheet is not sufficient to perform path integration as it results in ambiguities in location representations. Hence, multiple layers of neural sheet with various scales and orientations are required to encode unique locations in a space. Each neural sheet represents one grid cell population activity. In our implementation, λ and g_{exc} are uniformly sampled to generate multiple grid cell population activities. A hippocampal place cell population activity is defined as a weighted sum of a selective subset of grid cell population activities, i.e., a subset of neural sheets, with a global inhibition to balance the grid cell excitations:

$$p_i(r) = A\left[\sum_{j=1}^{N} w_{ij}^{eh} s_j(r) - C_{\text{inh}}\right]_+ \quad (5)$$

where A and C_{inh} are the gain and the global inhibition of the place cell network. N is the layers of neural sheet. w_{ij}^{eh} is the synaptic weight connecting from grid cell population activity j to place cell population activity i. r is the current location of the robot. C_{inh} affects the number of peaks by clustering the place cell population activities and is set as $B * max(p_i(r))$. B is used to control the peaks of the place cell population activities. To generate one major peak of the place cell population activities, we need to learn a synaptic weight distribution to determine a proportion of grid cell population activities with overlapping activity bumps at a single location (Si and Treves 2009; Savelli and Knierim 2010). This can be accomplished by either a linear summation of a subset of grid cells with certain spatial frequencies or Hebbian learning methods. Oscillatory interference based grid cell models are normally suitable for the linear summation method (Solstad, Moser, and Einevoll 2006). In this work, we instead apply competitive Hebbian learning to find a subset of CAN-based grid cell population activities to compute the corresponding place cell population activity for cognitive map building, as defined by:

$$dw_{ij}^{eh}/dt = kp_i(s_j - \langle s_j \rangle) \quad (6)$$

where k is the learning rate and $\langle\cdot\rangle$ is the mean of the grid cell activities. The learning rate k permits the formation of place cell population activities during the first few minutes of exploration. In our implementation, we set it as 0.00005 experimentally. In addition, we constrain $w_{ij}^{eh} \geq 0$ to prevent the weights becoming negative. Eq. (6) implicates that the sum over all weights is kept constant. Thus, small weights can be reduced by weight competition. According to the Oja's rule (Oja 1982), we further normalize the weights as $\sum_{j=1}^{N}(w_{ij}^{eh})^2 = 1$ to prevent the some neurons always winning the competition (Rolls, Stringer, and Elliot 2006).

The right-hand side of Eq. (6) determines the direction of weight changes: if the current grid cell population activity is greater than mean of the afferent population activities, the synapse is potentiated; otherwise, it is depressed. Eq. (6) allows to detect grid cell population activities with spatial coincidence from multiple layers of neural sheet. Figure 2 shows the evolution of the synaptic weights of the 80 layers of neural sheet during the first 5 minutes of the session. All the synaptic weights were initially assigned to $1/80$. It can be observed that by the competitive Hebbian learning algorithm, a small portion of the synaptic weights remained positive while a large portion of them converged to zero across the session. Thus, only a small subset of grid cell population activities will be selected to form one major peak of place cell population activities.

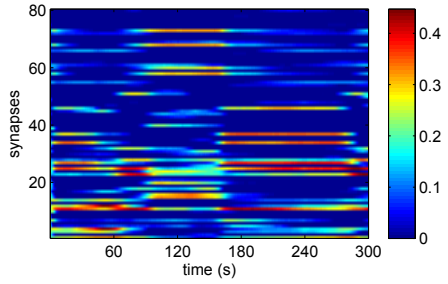

Figure 2: Evolution of synaptic weights.

Effects of Learning Parameters

In this section, we evaluate the effects of Hebbian learning parameters on place cell activities. Learning the synaptic weights between gird cells and place cells is important to determine the contributions of grid cell population activities to generating place cell population activities which encode the robot's locations for cognitive map building. The

size and the layers of neural sheets, the spacing of grid cell population activities in one neural sheet by λ and the gain g_{exc} mainly affect the formation of the place field activities. Obviously, if the value of λ increases, the spacing of the grid cells will also increases, thus leading fewer peaks of the place cell population activities. Fig 3 and 4 show how the size of neural sheet and the layers of neural sheet affect the learning results. In these two examples, g_{exc} is both set as 1.0. It can be observed that with the same λ and the layers of neural sheet, the larger the size of the neural sheet, the fewer the number of the major peaks of the place cell population activities. At the same time, with the same λ and the same size of the neural sheet, larger number of the the layers of neural sheet reduces the number of the major peaks of the place cell population activities.

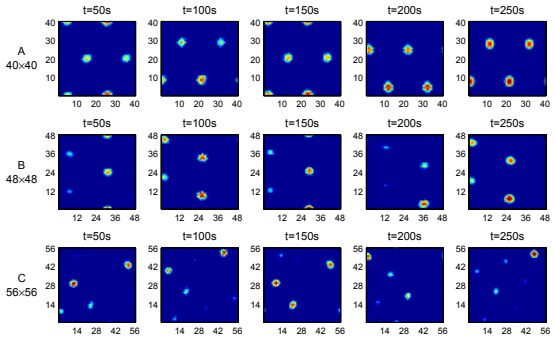

Figure 3: Larger size of the neural sheet leads to fewer peaks of the place cell population activities. Row A to C represent the results of 40×40, 48×48 and 56×56, respectively.

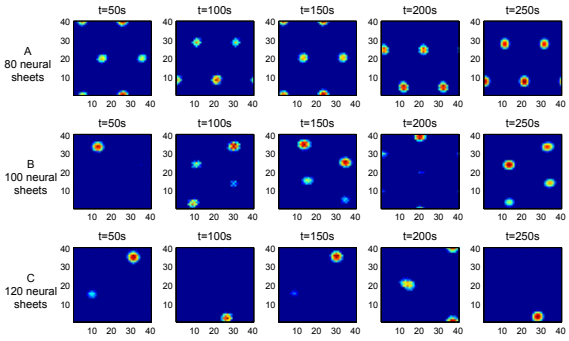

Figure 4: More grid cells reduce the number of the major peaks of the place cell population activities. Row A to C represent the results of 80, 100 and 120, respectively.

Different values of g_{exc} will also lead to different place cell population activities. Fig 5 shows the results in which g_{exc} was sampled from [1, 1.1]. It can be observed that the Hebbian learning results are much better than those when g_{exc} is set to 1.0, as shown in Row A in Fig 3 and 4. However, it is non-trivial to determine an optimum. In our current implementation, it was set experimentally. Furthermore, to deal with the presence of the multiple peaks, one solution is that we can increase the value of B to reduce the numbers

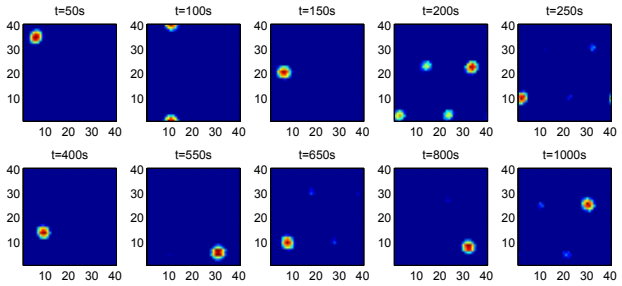

Figure 5: Place cell population activity generated from grid cell population activities with g_{exc} sampled from [1, 1.1].

of peaks. However, from our experiments, we have observed that the major peak of the place cell population activities exists consistently during the entire session even in the case of multiple peaks. Thus, this property of the proposed method guarantees that cognitive maps can be correctly built using various scales of grid cell networks.

Visual Calibration and Map Building

Evidence has revealed that when a rat returns to a familiar environment, the path integrator should be reset in order to adjust to the perceived environment (Moser, Kropff, and Moser 2008; Fuhs and Touretzky 2006). However, it remains unclear that how the brain senses and transforms external sensory inputs into an internal cognitive map (Burak and Fiete 2009). In our implementation, we use RGB-D images as visual cues to correct the path integration errors and reset the place cell population activities as well as the associated grid cell population activities at the previous locations and directions when loop closures are detected. Depth information can avoid ambiguity caused in 2D images and it is invariant to lighting conditions, in which many similar indoor scenes become distinguishable. A comparison between the image profiles is performed for each pair of incoming RGB and depth frames (Tian et al. 2013) for loop closure and new scene detection.

Our cognitive map contains a set of spatial coordinates that the robot has experienced in its past travels, as shown in Fig 6. The robot's spatial coordinates are calculated from the place cell population activities which are generated from a subset of grid cell population activities using Eq. (5). Nodes in the cognitive map are constructed by associating the major peak of the place cell population activities with corresponding visual cues, locations and denoted as visual experiences. These visual experiences serve as visual cues for loop closure detection. **Algorithm** 1 shows the cognitive map building process. The incoming visual inputs are compared with the historical visual experiences. If the latest input matches the previous visual experiences, it is considered as a familiar scene which had been seen previously by the robot. The status of the grid cell population activities and the place cell population activity are then reset to the previous matched visual experiences. The current visual input and the matched visual experience are merged to one experience. Otherwise, a new visual experience is created. Once

a loop closure is detected, the map will be adjusted to the recalled visual experiences.

Algorithm 1: The Cognitive Map Building Algorithm

Input: Raw odometry data from the robot wheel encoders and visual images from the RGB-D sensor
Output: Cognitive map
Begin:
- Calculate grid cell population activities using Eq. (1)-(4).
- Calculate place cell population activities using Eq. (5).
- Obtain one major peak of place cell population activities using Eq. (6).
- Perform visual profile comparison.
  if The incoming visual input matches the previous visual experiences,
  then Perform resetting and map correction.
  else Create a new visual experience.
  end if

End:

Experimental Analysis

We aim to build a cognitive map for a large office environment of $35m \times 35m$ on a mobile robot to validate the effectiveness of the proposed model. Table shows the parameters setting. The mobile robot is commanded to make a complete exploration of the indoor environment (the exploration process is shown in the accompanying video).

Fig.6 shows the experimental results. Row A shows the dead-reckoning map obtained from the robot odometry. Obviously, this map can not represent the environment properly. Row B shows the cognitive map built by the proposed computational model. With visual inputs, the system can successfully perform loop closure detection and and correct the odometry drift. Finally it generates a cognitive map which encodes both topological and metric information. In Row C, the blue dotted line shows the real trajectory traveled by the robot, and the red crosses indicate the firing locations of the grid cell located at (20,20) in the 21^{th} layer of the neural sheets. Row D shows the corresponding rate map. To generate the rate map, a spatial smoothing algorithm using a Gaussian kernel, as described in (Hafting et al. 2005), is adopted with a bin size of $0.5m \times 0.5m$.

From the experiment, we have observed that before the first loop closure was detected, the cognitive map was the same as the raw map built directly using the raw odometry data. When the loop closure was detected (i.e., the robot detected a scene which it had traveled.), resetting was performed and the map was corrected according to the recalled visual experiences. Fig. 7 demonstrates an example of loop closure detection and path integration resetting process. Fig. 7(a) and (b) show the constructed map and corresponding place cell population activities at t=15 seconds. When t=265 seconds, the incoming visual input matched with the previous visual experience (t=15 seconds) and a loop closure was thus detected (Fig. 7(c)). Immediately, the system corrected the map (at t=267.5 seconds), as shown in Fig. 7(e). Correspondingly, the grid cell population activities and the place cell population activities were reset to the visual experience at t=15 seconds. Fig. 7(f) show the result of resetting the place cell population activities at t=265 seconds (Fig. 7(d)) to the previous position and direction of the visual experience at t=15 seconds (Fig. 7(b))[1]. It should be noted that the positions of the place cell population activities in Fig. 7(b), (d) and (f) are not the same as those in the cognitive map because the place cell population activities only encoded the robot's relative positions. In addition, before and after the resetting process, the synaptic weights remained unchanged, thus resulting in different activities at t=15 seconds and 267.5 seconds. As observed, the final raw maps built directly using the raw odometry data failed to represent the real environment due to the accumulated errors, while the cognitive maps built using path integration resetting correctly represented the environment with associated visual experiences. Fig. 8 shows that the final cognitive map correctly represented the spatial representation of the robot's exploring space.

Parameter	Setting
Shift in Outgoing Weights l	2
Size of Neural Sheet	40×40
Time-Constant of Neuron Response τ	10ms
Periodicity of the Formed Lattice λ	[13, 21]
Gain g_{exc}	[1, 1.1]
Parameter B	0.5
Layers of Neural Sheet N	80
Learning Rate k	0.00005

Table 1: Parameter Setting

Throughout the map building process, the grid cells spiked at regular intervals along the robot trajectory, displaying grid-like property. Compared to the regularly tessellating triangle structure spanning the environment observed from the grid cells in rat's entorhinal cortex region (Hafting et al. 2005), the responses of a single grid cell in our simulation were at regular intervals because the robot explored the environments with guided exploration in order to build a complete map.

Discussion

As addressed above, place cell activities are generated from a selected subset of grid cell activities. In a recent research (Bonnevie et al. 2013), it is found that the formation of grid cells is also dependent on place cells by hippocampal backprojections. In our model, grid cells interact with place cells. First, due to the ambiguous location representations in grid cells, the resetting process was performed on place cells, leading to the corresponding resettings of grid cells. Second, the competitive Hebbian learning used in this work also implicates that grid cells interact with place cells.

In most existing experiments (Burak and Fiete 2009; Zilli and Hasselmo 2010), the velocity inputs are extracted from ground-truth trajectories recorded by an allothetic tracking system. However, for animals or autonomous mobile robots, the accumulated errors are inevitable. In our model, the velocity inputs were extracted from idiothetic wheel encoders,

[1]The resetting results of grid cells are not shown in the paper.

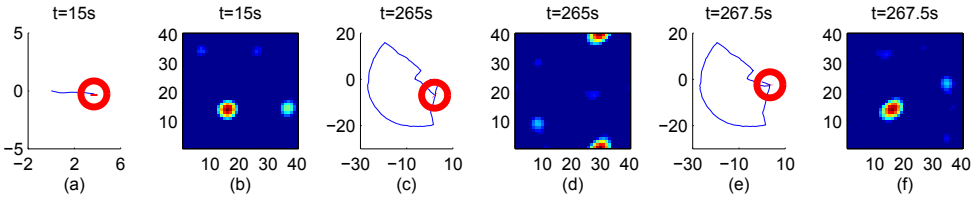

Figure 7: Loop closure detection and path integration resetting. The red circle indicates the robot's current position.

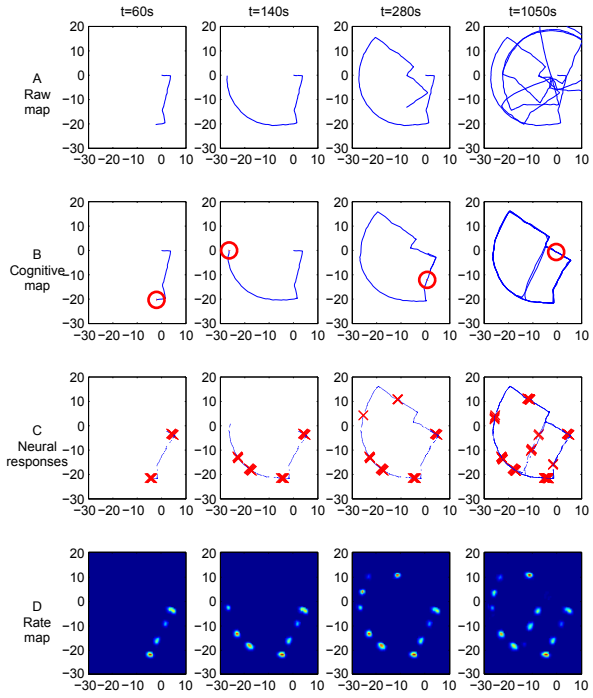

Figure 6: Neural responses in the map building process.

Figure 8: The final cognitive map (in blue) superimposed on the office layout.

which are self-generated signals and the accumulated errors are reflected in raw odometry data, to generate and drive CAN-based grid cell population activities. Together with the visual information captured from the RGB-D sensor for loop closure detection and map correction, our cognitive map model is able to produce accurate representation of the environment in contrast to what constructed from the raw data.

Neural Sheet	Memory(MB)	Time (Second)
32×32	66	450
40×40	217	1638
48×48	564	2304
56×56	1180	10913
64×64	2192	21988

Table 2: Weights for various neural sheets

For computational efficiency, we use a small scale network with a sheet of 40×40 neurons and N is 80. We have conducted experiments with large scale of grid cell networks, such as 64×64, which can still build accurate cognitive maps. However, it is found that the CAN-based grid cell model is computationally inefficient and not scalable. With larger n, the generation time and the memory storage of the recurrent synaptic weights increase dramatically. Table shows the times and memories to generate and store the recurrent synaptic weights of 80 layers of neural sheet with various sizes of the neural sheet. It can be seen that for only 80 grid cell population activities with a sheet of 64×64, it requires around 6 hours to generate and 2.2G memory to store the recurrent synaptic weights. To simulate large scale networks, using scalable neuromorphic hardware (Furber et al. 2014; Merolla et al. 2014) could drive the way.

Our cognitive map model will contribute to developing innovative robotic spatial cognition approaches (Huang, Tang, and Tian 2014; Milford, Wiles, and Wyeth 2010). Compared to the traditional probabilistic SLAM algorithms, the proposed method tracks the neural activities, which encode locations and orientations with regard to the robot in a cognitive map. The advantage is that poses and related view information can be efficiently associated with the cognitive map for efficient robot navigation and localization without modeling uncertainties of landmarks.

Conclusion

In this paper, we proposed a novel entorhinal-hippocampal model which is able to build cognitive maps simultaneously by integrating activities of place cells and grid cells with real visual inputs. The mobile robot embedded with the spatial cognitive model was able to accurately map the environment. Such a model will facilitate to investigate neural mechanisms of spatial cognition in a non-intrusive way. Furthermore, it will inspire innovative robotic approaches for mapping, localization and navigation, etc.

References

Bonnevie, T.; Dunn, B.; Fyhn, M.; Hafting, T.; Derdikman, D.; Kubie, J. L.; Roudi, Y.; Moser, E. I.; and Moser, M.-B. 2013. Grid cells require excitatory drive from the hippocampus. *Nature neuroscience* 16(3):309–317.

Burak, Y., and Fiete, I. R. 2009. Accurate path integration in continuous attractor network models of grid cells. *PLoS computational biology* 5(2):e1000291.

Burgess, N.; Donnett, J. G.; Jeffery, K. J.; John, O.; et al. 1997. Robotic and neuronal simulation of the hippocampus and rat navigation. *Philosophical Transactions of the Royal Society of London. Series B: Biological Sciences* 352(1360):1535–1543.

Burgess, N. 2008. Grid cells and theta as oscillatory interference: theory and predictions. *Hippocampus* 18(12):1157–1174.

Cuperlier, N.; Quoy, M.; and Gaussier, P. 2007. Neurobiologically inspired mobile robot navigation and planning. *Frontiers in neurorobotics* 1.

Domnisoru, C.; Kinkhabwala, A. A.; and Tank, D. W. 2013. Membrane potential dynamics of grid cells. *Nature* 495(7440):199–204.

Fuhs, M. C., and Touretzky, D. S. 2006. A spin glass model of path integration in rat medial entorhinal cortex. *The Journal of Neuroscience* 26(16):4266–4276.

Furber, S. B.; Galluppi, F.; Temple, S.; and Plana, L. A. 2014. The spinnaker project. *Proceedings of the IEEE* 102(5):652–665.

Hafting, T.; Fyhn, M.; Molden, S.; Moser, M.-B.; and Moser, E. I. 2005. Microstructure of a spatial map in the entorhinal cortex. *Nature* 436(7052):801–806.

Huang, W.; Tang, H.; and Tian, B. 2014. Vision enhanced neuro-cognitive structure for robotic spatial cognition. *Neurocomputing* 129:49–58.

Jauffret, A.; Cuperlier, N.; and Gaussier, P. 2012. Multimodal integration of visual place cells and grid cells for robots navigation. In *Second Symposium on Biology of Decision Making*, 136–145.

McNaughton, B. L.; Battaglia, F. P.; Jensen, O.; Moser, E. I.; and Moser, M.-B. 2006. Path integration and the neural basis of the'cognitive map'. *Nature Reviews Neuroscience* 7(8):663–678.

Merolla, P. A.; Arthur, J. V.; Alvarez-Icaza, R.; Cassidy, A. S.; Sawada, J.; Akopyan, F.; Jackson, B. L.; Imam, N.; Guo, C.; Nakamura, Y.; Brezzo, B.; Vo, I.; Esser, S. K.; Appuswamy, R.; Taba, B.; Amir, A.; Flickner, M. D.; Risk, W. P.; Manohar, R.; and Modha, D. S. 2014. A million spiking-neuron integrated circuit with a scalable communication network and interface. *Science* 345(6197):668–673.

Milford, M., and Wyeth, G. 2008. Mapping a suburb with a single camera using a biologically inspired slam system. *Robotics, IEEE Transactions on* 24(5):1038–1053.

Milford, M. J.; Wiles, J.; and Wyeth, G. F. 2010. Solving navigational uncertainty using grid cells on robots. *PLoS computational biology* 6(11):e1000995.

Monaco, J. D., and Abbott, L. F. 2011. Modular realignment of entorhinal grid cell activity as a basis for hippocampal remapping. *The Journal of Neuroscience* 31(25):9414–9425.

Moser, E. I.; Kropff, E.; and Moser, M.-B. 2008. Place cells, grid cells, and the brain's spatial representation system. *Neuroscience* 31(1):69.

Oja, E. 1982. Simplified neuron model as a principal component analyzer. *Journal of mathematical biology* 15(3):267–273.

O'Keefe, J., and Dostrovsky, J. 1971. The hippocampus as a spatial map. preliminary evidence from unit activity in the freely-moving rat. *Brain research* 34(1):171–175.

O'keefe, J., and Nadel, L. 1978. *The hippocampus as a cognitive map*, volume 3. Clarendon Press Oxford.

Rolls, E. T.; Stringer, S. M.; and Elliot, T. 2006. Entorhinal cortex grid cells can map to hippocampal place cells by competitive learning. *Network: Computation in Neural Systems* 17(4):447–465.

Savelli, F., and Knierim, J. J. 2010. Hebbian analysis of the transformation of medial entorhinal grid-cell inputs to hippocampal place fields. *Journal of neurophysiology* 103(6):3167–3183.

Si, B., and Treves, A. 2009. The role of competitive learning in the generation of dg fields from ec inputs. *Cognitive neurodynamics* 3(2):177–187.

Solstad, T.; Moser, E. I.; and Einevoll, G. T. 2006. From grid cells to place cells: a mathematical model. *Hippocampus* 16(12):1026–1031.

Taube, J. S. 2007. The head direction signal: origins and sensory-motor integration. *Annu. Rev. Neurosci.* 30:181–207.

Tian, B.; Shim, V. A.; Yuan, M.; Srinivasan, C.; Tang, H.; and Li, H. 2013. Rgb-d based cognitive map building and navigation. In *Intelligent Robots and Systems (IROS), 2013 IEEE/RSJ International Conference on*, 1562–1567. IEEE.

Tolman, E. C. 1948. Cognitive maps in rats and men. *Psychological review* 55(4):189.

Zhang, K. 1996. Representation of spatial orientation by the intrinsic dynamics of the head-direction cell ensemble: a theory. *The journal of neuroscience* 16(6):2112–2126.

Zilli, E. A., and Hasselmo, M. E. 2010. Coupled noisy spiking neurons as velocity-controlled oscillators in a model of grid cell spatial firing. *The Journal of neuroscience* 30(41):13850–13860.